DNA folding and melting observed in real time redefine the energy landscape

Hairong Ma, Chaozhi Wan, Aiguo Wu, and Ahmed H. Zewail*

Physical Biology Center for Ultrafast Science and Technology and Laboratory for Molecular Sciences, California Institute of Technology, Pasadena, CA 91125

Contributed by Ahmed H. Zewail, November 13, 2006 (sent for review November 1, 2006)

We report real-time observations of the folding and melting of DNA by probing two active sites of a hairpin structure, the bases and the stem end, and using an ultrafast *T*-jump. Studies at different initial temperatures (before, during, and after melting) provide the time scale of water heating (<20 ps), single-strand destacking (700 ps to 2 ns), and hairpin destacking (microseconds and longer) in solutions of various ionic strengths and pH values. The behavior of transient changes gives direct evidence to the existence of intermediate collapsed structures, labile in destacking but compact in nature, and indicates that melting is not a two-state process. We propose a landscape that is defined by these nucleation structures and destacking for efficient folding and melting.

biopolymers | macromolecular folding | ultrafast *T*-jump

The folding of a biomolecule is an inherently complex process involving an energy landscape that describes the possible conformations and nuclear/segment motions (1–7). Different time scales (8–10) are involved and span the slow, large-amplitude motions and fast, local motions. The former is the rate-limiting step in the folding process and involves the passage through basins and barriers of the energy surface, ultimately reaching the final native structure. In contrast, elementary local motions are those of structures that may or may not be transient intermediates; their existence is critical to the description of the pathways and rates of folding and melting. Such elementary motions are often hidden from detection when the time resolution used is relatively long. Much work has been done on protein folding and their energy landscapes. For DNA and RNA, the melting problem (11) is usually identified in textbooks by two states:

$$\text{folded state } (F) \rightleftharpoons \text{unfolded state } (U); \qquad [1]$$

however, recent reports (12–14) have suggested the existence of intermediates for hairpin nucleic acids from experiments with ≈10-ns or longer time resolution.

To directly observe the elementary processes of folding and melting, we invoked the methodology of a *T*-jump with an ultrashort time resolution that reaches the thermal limit of water heating (15). The system is perturbed to a nonequilibrium state, and its relaxation toward a new equilibrium state is monitored in real time by using a probe pulse. We use two active sites for probing: the actual base dynamics through the evolution of the hypochromicity of bases and the stem-end degree of folding through the evolution of a fluorescence marker (Fig. 1). The observations were made in the time window of picoseconds to nanoseconds at different initial temperatures (before, during, and after melting) and for solutions of various pH values and ionic strengths (buffer, water, and sodium hydroxide). The hairpin secondary structure, besides being the building block of tertiary structures, also is important in biological function, e.g., folding initiation, ligand binding, and replication and transcription (16, 17).

Results and Discussion

Melting at Steady State. Because UV absorbance increases upon destacking, the so-called hypochromic effect, a rise in temperature causes an increase in absorbance due to loss of stacking (18). The thermal titration curves of Fig. 2 *a* and *c* show the sigmoidal "melting curves" for DNA with the transition normally attributed to a two-state melting model; the changes in absorption and fluoresence spectra are shown in Fig. 2 *b* and *d*. For this hairpin sequence, the melting temperature in water was found to be ≈15°C lower than that in the buffer, indicating that the highly charged DNA backbone is somewhat destabilized due to the lack of counterions (19). In contrast, in the sodium hydroxide solution, a nearly linear temperature response with no transition was observed. As it is well known, in such a denaturing solution the hairpin conformation becomes much less stable, providing a medium for the probing of extended single-strand structures.

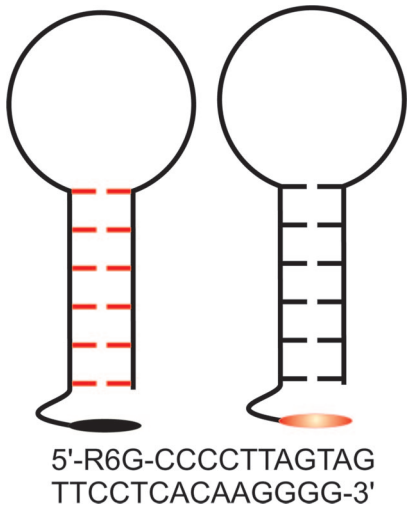

Fig. 1. A schematic of the oligonucleotide hairpin structure (25 residues) used in this study. A fluorescence marker (R6G dye) is attached to the 5′ end of the strand. The probing of the base (*Left*) and stem-end (*Right*) conformational changes is highlighted. The sequence of the oligonucleotide is shown below the markers.

The absorption experiments are blind to the local conformation of the stem end. In the hairpin structure, where end-to-end contacts are formed, the marker is nearly stacked with a guanine residue at the opposite end. Because of electron transfer, the fluorescence is greatly quenched when the ends stack and is recovered when they are far apart (20). Thus, the fluorescence intensity increases with temperature, as we observed experimentally. Similar to the behavior observed by probing the bases in buffer and water solutions, the stem end of the hairpin undergoes

Author contributions: H.M., C.W., A.W., and A.H.Z. performed research and H.M., C.W., and A.H.Z. wrote the paper.

The authors declare no conflict of interest.

Freely available online through the PNAS open access option.

*To whom correspondence should be addressed. E-mail: zewail@caltech.edu.

www.pnas.org/cgi/doi/10.1073/pnas.0610028104

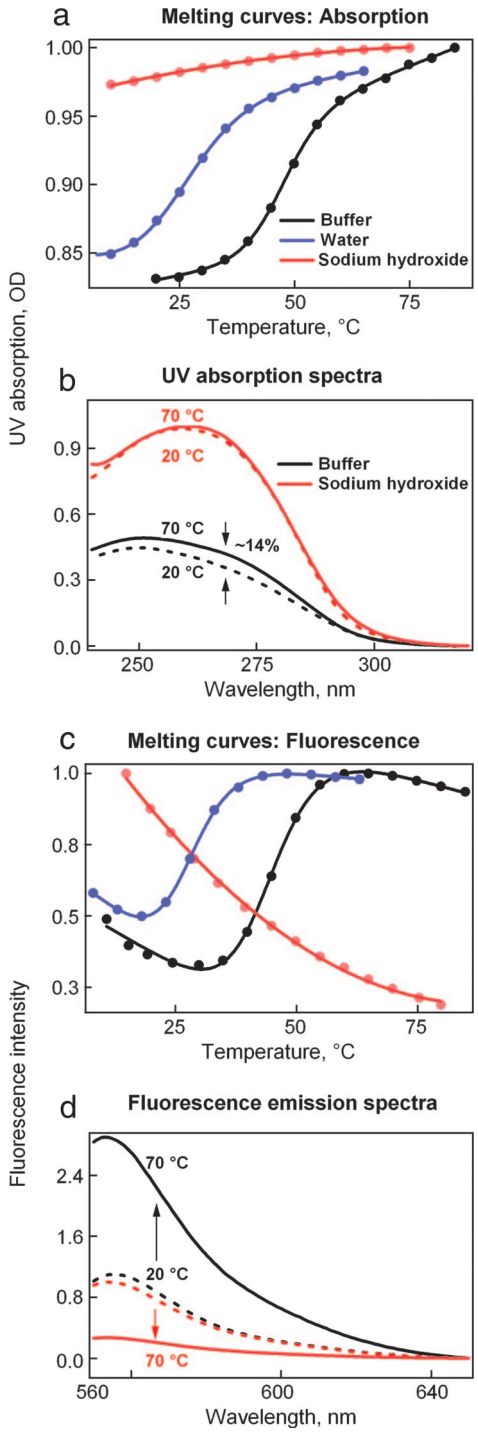

Fig. 2. Melting curves and spectra of the DNA hairpin. (*a*) Measured UV absorptivity at different conditions: salt buffer (50 mM Na^+/30 mM phosphate, pH 7); Barnstead Nanopure water (18 MΩ); and sodium hydroxide solution (1 M). (*b*) UV absorption spectra of DNA in different solutions and at different temperatures (20°C and 70°C). (*c*) Fluorescence of the marker (excitation at 530 nm) in different solutions. The fluorescence intensity is integrated from 550 to 650 nm. (*d*) Fluorescence emission spectra (excitation at 530 nm) of different solutions and at different temperatures. In *a* and *c*, the melting curves are fitted to a two-state model for DNA in water and the buffer; in sodium hydroxide solutions, the curves connecting the experimental points only serve to guide the eye. The melting curves and spectra are scaled for a better view.

an apparent two-state transition; whereas in sodium hydroxide the DNA molecules are in the unfolded state. We note that the fluorescence of the marker decreases as temperature increases,

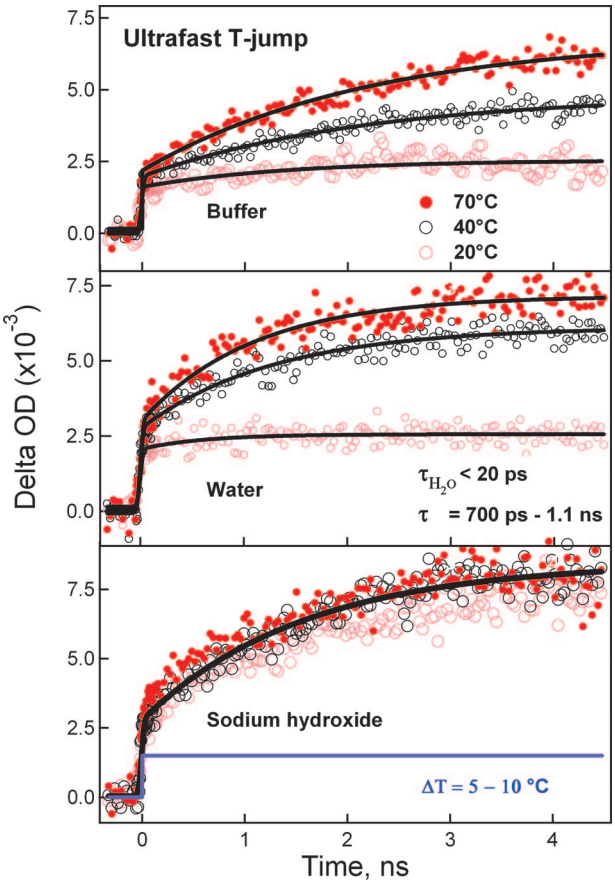

Fig. 3. Transient evolution of hypochromicity of the oligonucleotides after the ultrafast *T*-jump, measured for different solutions and three initial temperatures. The filled and empty circles represent experimental data, and the smooth curves are the best fits to a deconvoluted single-exponential function. The *T*-jump also is illustrated (blue line) in the bottom graph.

due to the decreased polarity by cytosine's shielding at lower temperatures; when titrating free R6G with cytosine we observed similar behavior.

Base Destacking Dynamics. For dynamic studies, we first performed measurements of the UV transient absorption of the bases by using a probe pulse at 266 nm and after an ultrafast *T*-jump at the 1.5-μm energy absorbed by the water molecules. We performed numerous experiments of this kind; Fig. 3 summarizes the results for three temperatures and three solutions. The temperature jump was calibrated (15), and here we used up to 10°C *T*-jump to probe the transition region. For all initial temperatures, the temporal response shows two rising components over a time scale of 4.8 ns. An ultrafast rise (<20 ps) describes the desolvation process initiated by the *T*-jump, the picosecond rotational and translational motions of the water heated up (15). The other component is on a longer time scale, and its rise with time indicates that the bases become less stacked after the *T*-jump, consistent with the observed trend of hypochromicity at steady state. In water solution, the rise time ranges from 700 ps to 1.1 ns, whereas rise times in the buffer and sodium hydroxide are ≈2.1 ns and ≈1.5 ns, respectively, all of which are in the postmelting regime (70°C).

For an initial temperature far below the transition temperature (≈50°C in the buffer and ≈35°C in water), the *T*-jump does not result in a rise of absorbance, whereas at 40°C and 70°C the rise is clear, with a larger amplitude for the latter. Therefore, it

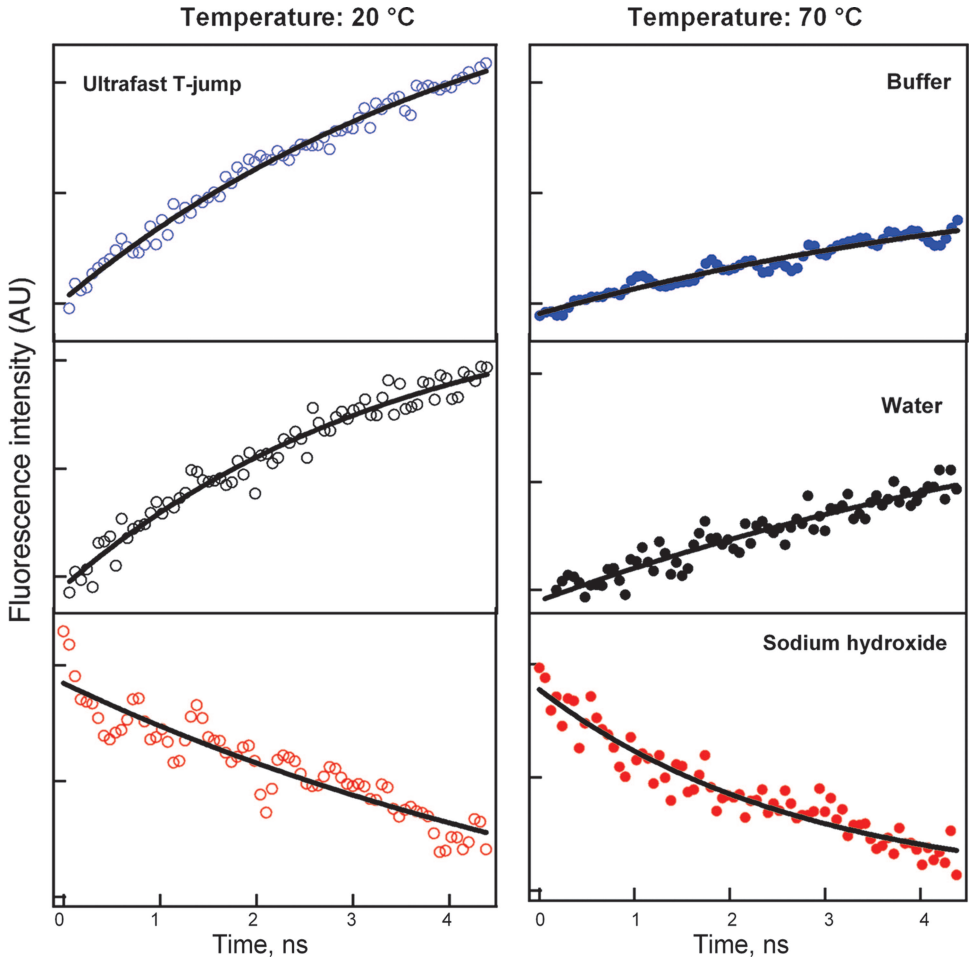

Fig. 4. Transient evolution of the fluorescence marker after the *T*-jump, measured for different solutions and for three initial temperatures. The excitation is at 530 nm, and the intensity is collected with a 550-nm, long-pass filter. The filled and empty circles represent experimental data, and the smooth curves are the best fits to a single-exponential function. In water and buffer solutions, the amplitudes are to scale, whereas, in sodium hydroxide, the amplitudes are normalized.

is evident that the (nanosecond) rise is due to the destacking dynamics of single strands and that the destacking of the hairpin occurs on a much longer time scale (microseconds), consistent with a larger stabilization energy for the hairpin; the energy barrier is > 8 kcal/mol for the opening/closing of a double helix (21, 22). Furthermore, the increase in rise time upon going from the water to the buffer is correlated with the stability due to an increase in ionic strength.

Further support of the time scale for destacking in melted structure comes from the changes in amplitude observed at different initial temperatures and in different solutions. The relative transient amplitudes are nearly independent of the initial temperature in sodium hydroxide, whereas the transient shows a higher relative amplitude in water ($\approx$70%) than in buffer ($\approx$50%) at 40°C. These trends indicate that base destacking occurs at a lower initial temperature in water and that melted chains are responsible for the observed transients. It is significant that the time scale involved in destacking dynamics of single strands is at least two orders of magnitude shorter than that of double helix structures (8, 23). It is, however, consistent with the time range ($\approx$1 ns) deduced for local structural elements rearrangement of a free chain (10).

Stem-End Motion. In contrast to UV transient absorption, which detects stacking motions, time-resolved fluorescence of the marker is sensitive to local conformational changes near the stem end. As mentioned above for the hairpin structure, the marker fluorescence must increase after the *T*-jump as the structure extends into single strands. Consistent with this picture, in Fig. 4, the observed transients (fluorescence detection) display a rise (fluorescence increase) in buffer and water solutions but show a decay (fluorescence decrease) in sodium hydroxide; the time constant is $\approx$5 ns.

The most striking observation is the unexpected increase in fluorescence in the postmelting regime at 70°C for the buffer and water solutions. We expected the hairpin and single-stranded structure to have opposite behavior after the *T*-jump: a rise of the fluorescence with time for the former structure and a decrease of the fluorescence with time for the latter. Indeed, in sodium hydroxide solution, a decay was observed for all temperatures studied. In buffer and water, if the melting transition process can truly be expressed by a two-state model, the steady state sigmoidal behavior gives the hairpin structure population to be $>$70% at 20°C and $<$5% at 70°C. Because of this change in population at the two temperatures, the dynamics should show a dramatic opposite change, but, surprisingly, such a change was not observed here; only a rising signal is detected. The fluorescence relaxation at 70°C resembles the one at 20°C, retaining $\approx$30% of the amplitude.

The transient fluorescence results indicate the existence of a new intermediate melted state with a collapsed structure where the marker is still in contact with the guanine residue at the other

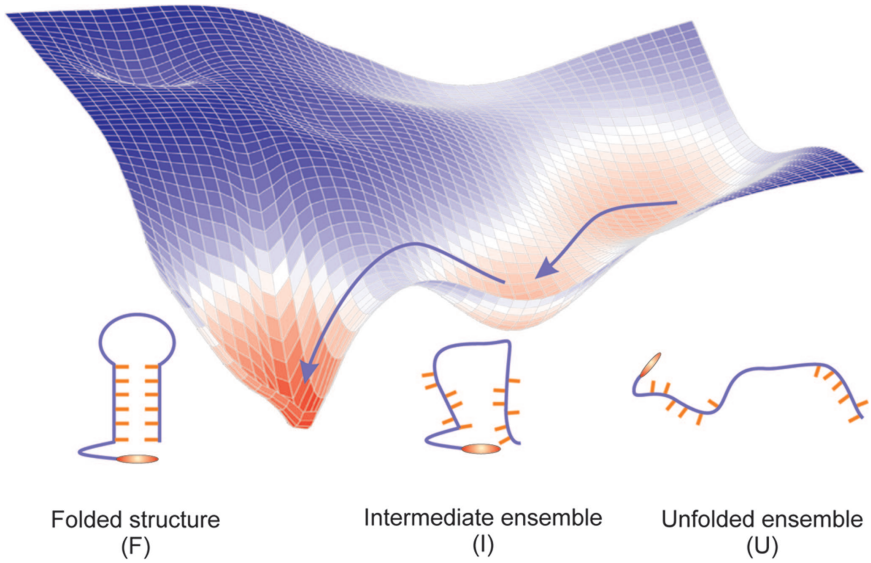

Fig. 5. The landscape picture for DNA hairpin folding and melting. The free-energy surface with multiple global minima depicts folded, collapsed (compact) intermediate, and single-stranded structures. A schematic of the different structures is also shown.

end. Such a collapsed structure will not be detected in the steady-state melting curves because of the insensitivity to partially unfolded species in solution. Even the UV transient experiments will not reveal the difference between the collapsed and extended single-strand state. It should be mentioned that, for the DNA sequence we used here, thermodynamic calculations of melting (24) suggest that the self-complementary duplex structure is much less stable than the hairpin conformation and has a lower melting temperature by ≈20°C, which is contrary to the observations made in Fig. 2. Furthermore, steady-state experiments at different concentrations did not show evidence of a concentration-dependent melting behavior. Accordingly, the dynamics contributed by the duplexes are negligible.

Melting and Folding Landscape. Given the observations reported here, we are in a position to suggest the landscape picture for melting and folding (Fig. 5). The process at the molecular level involves two types of structures, both of which are partially stacked, but one is extended and the other is a compact collapsed structure. The collapsed intermediate is stable because its population (≈30%) on our observed nanosecond time scale is unlikely from the folded state (high energy barrier; microsecond time scale) or from the unfolded extended state because it requires an intrachain diffusion on the microsecond time scale. We estimated this diffusion time, as done for polypeptides (25), by using the Szabo, Schulten, and Schulten theory (26, 27). The destacking dynamics, with its nanosecond time scale, represents another coordinate of the landscape and is a facilitator of structural changes. The compact intermediate is a "nucleation site" on the energy landscape for a whole family of conformations. This nucleation greatly reduces the configurational space and thus allows for an efficient search of the native structure.

The biological significance of the observed time scales and intermediate structures can perhaps be summarized in the following points. First, the time scale of water reorientation is indeed ultrafast (<20 ps), but that of destacking in a single strand is ≈1 ns, which in turn is at least three orders of magnitude faster than that of the hairpin. The ≈1-ns time scale is interestingly similar to that of small segment torsional motions (28, 29), but more importantly it is short enough, on the time scale of global motions, to allow for the reduction of internal friction and the optimization of cooperativity in folding. Second, melting is not strictly a two-state process, and the identification of a collapsed (end-to-end contact) structure in the postmelting regime, with destacking mobility, indicates that the search for the native structure is designed for an effective pathway and rate of folding. Finally, these structures relate to those identified as "premelting states" (30) in that they have the capability to function as efficient binding sites for drugs or enzymes. These structures could not be observed with previous methods using slower time resolution or at steady state.

The above three-state picture of melting and folding raises some new questions. The role of the solvent on the picosecond time scale is significant and raises the issue of its involvement. It is possible that the fast motion of water molecules is a doorway-aiding process for forming the intermediate ensemble from the configurations of unfolded structures. This formation process would be analogous to the slaving of protein folding by solvent motion, primarily by the dielectric relaxation of bulk solvent on the time scale of $\approx 10^{-11}$ sec (31). Another issue is the thermodynamics and kinetics of relatively small systems (32). How sharp should the transition be in a finite system? Because the free energy difference is the product of the number of particles involved and difference in chemical potential, the coexistence of more than two states in melting is possible for small systems. And, finally, one must ask the question raised more than 30 years ago: What is the nature of phase transitions with end effects (33) in such biopolymers? Stimulated by the experimental results reported here, theoretical models of helix-to-coil transitions with specific microscopic structural motifs and dynamics can now be developed, together with experiments for the study of these transitions in proteins (34, 35) using our ultrafast *T*-jump.

Materials and Methods

The 25-nt DNA strand studied here is a synthesized oligonucleotide that readily forms a hairpin under physiological conditions. The complimentary bases on both ends (5′-CCCCAA and TTGGGG-3′) form a double helix stem, and the other residues in the middle of the strand form a loop (Fig. 1); the marker (R6G dye) is at the 5′ position for the same sequence (20). The experimental apparatus is detailed in ref. 15.

This work was supported by the National Science Foundation and the Physical Biology Center for Ultrafast Science and Technology.

1. Wolynes PG, Onuchic JN, Thirumalai D (1995) *Science* 267:1619–1620.
2. Onuchic JN, Wolynes PG (2004) *Curr Opin Struct Biol* 14:70–75.
3. Dobson CM (2003) *Nature* 426:884–890.
4. McMillon PF, Clary DC, eds (2005) *Philos Trans A* 363:309–607.
5. Frauenfelder H, McMahon BH (2000) *Annal Phys* 9:655–667.
6. Gruebele M (2005) *Comp Rend Biol* 328:701–712.
7. Fersht AR (1999) *Structure and Mechanism in Protein Science: A Guide to Enzyme Catalysis and Protein Folding* (Freeman, New York).
8. Crothers DM (2001) in *RNA*, eds Soll D, Nishimura S, Moore PB (Pergamon/Elservier, Oxford), pp 61–70.
9. Crothers DM (1969) *Acc Chem Res* 2:225–232.
10. McCammon JA, Harvey SC (1987) *Dynamics of Proteins and Nucleic Acids* (Cambridge Univ Press, New York).
11. Tinoco I, Sauer K, Wang JC, Puglisi JD (2002) *Physical Chemistry: Principles and Applications in Biological Sciences* (Prentice–Hall, Englewood Cliffs, NJ).
12. Ma HR, Proctor DJ, Kierzek E, Kierzek R, Bevilacqua PC, Gruebele M (2006) *J Am Chem Soc* 128:1523–1530.
13. Jung JY, Van Orden A (2006) *J Am Chem Soc* 128:1240–1249.
14. Goddard NL, Bonnet G, Krichevsky O, Libchaber A (2000) *Phys Rev Lett* 85:2400–2403.
15. Ma HR, Wan CZ, Zewail AH (2006) *J Am Chem Soc* 128:6338–6340.
16. Tinoco I, Bustamante C (1999) *J Mol Biol* 293:271–281.
17. Varani G (1995) *Annu Rev Biophys Biomol Struct* 24:379–404.
18. Norberg J, Nilsson L (1995) *J Phys Chem* 99:13056–13058.
19. Tan ZJ, Chen SJ (2006) *Biophys J* 90:1175–1190.
20. Heinlein T, Knemeyer JP, Piestert O, Sauer M (2003) *J Phys Chem B* 107:7957–7964.
21. Ramstein J, Lavery R (1988) *Proc Natl Acad Sci USA* 85:7231–7235.
22. Xu DG, Evans KO, Nordlund TM (1994) *Biochemistry* 33:9592–9599.
23. Porschke D (1976) *Biochemistry* 15:1495–1499.
24. Borer PN, Dengler B, Tinoco I, Uhlenbec OC (1974) *J Mol Biol* 86:843–853.
25. Lapidus LJ, Eaton WA, Hofrichter J (2000) *Proc Natl Acad Sci USA* 97:7220–7225.
26. Szabo A, Schulten K, Schulten Z (1980) *J Chem Phys* 72:4350–4357.
27. Zhou HX (2003) *J Chem Phys* 118:2010–2015.
28. Millar DP, Robbins RJ, Zewail AH (1980) *Proc Natl Acad Sci USA* 77:5593–5597.
29. Allison SA, Schurr JM (1979) *Chem Phys* 41:35–59.
30. Chan SS, Breslauer KJ, Hogan ME, Kessler DJ, Austin RH, Ojemann J, Passner JM, Wiles NC (1990) *Biochemistry* 29:6161–6171.
31. Frauenfelder H, Fenimore PW, Chen G, McMahon BH (2006) *Proc Natl Acad Sci USA* 103:15469–15472.
32. Berry RS (2002) in *Strength from Weakness: Structural Consequences of Weak Interactions in Molecular, Supermolecules, and Crystals*, eds Domenicano A, Hargittai I (Kluwer Academic, Dordrecht, The Netherlands), pp 143–168.
33. Sture K, Nordholm J, Rice SA (1973) *J Chem Phys* 59:5605–5614.
34. Schuler B, Lipman EA, Eaton WA (2002) *Nature* 419:743–747.
35. Rhoades E, Cohen M, Schuler B, Haran G (2004) *J Am Chem Soc* 126:14686–14687.